materials

MDPI

Article

Mechanical and Thermal Conductivity Properties of Enhanced Phases in Mg-Zn-Zr System from First Principles

Shuo Wang, Yuhong Zhao *, Huijun Guo, Feifei Lan and Hua Hou

School of Materials Science and Engineering, North University of China, Taiyuan 030051, China; wangshuo313@sina.cn (S.W.); ghjwwd@163.com (H.G.); lan.feifei@foxmail.com (F.L.); houhua@nuc.edu.cn (H.H.)

* Correspondence: zhaoyuhong@nuc.edu.cn; Tel.: +86-150-3517-2958

Received: 25 September 2018; Accepted: 15 October 2018; Published: 17 October 2018

Abstract: In this paper, the mechanical properties and minimum thermal conductivity of ZnZr, Zn_2Zr, Zn_2Zr_3, and $MgZn_2$ are calculated from first principles. The results show that the considered Zn-Zr intermetallic compounds are effective strengthening phases compared to $MgZn_2$ based on the calculated elastic constants and polycrystalline bulk modulus B, shear modulus G, and Young's modulus E. Meanwhile, the strong Zn-Zr ionic bondings in ZnZr, Zn_2Zr, and Zn_2Zr_3 alloys lead to the characteristics of a higher modulus but lower ductility than the $MgZn_2$ alloy. The minimum thermal conductivity of ZnZr, Zn_2Zr, Zn_2Zr_3, and $MgZn_2$ is 0.48, 0.67, 0.68, and 0.49 W m^{-1} K^{-1}, respectively, indicating that the thermal conductivity of the Mg-Zn-Zr alloy could be improved as the precipitation of Zn atoms from the α-Mg matrix to form the considered Zn-Zr binary alloys. Based on the analysis of the directional dependence of the minimum thermal conductivity, the minimum thermal conductivity in the direction of [110] can be identified as a crucial short limit for the considered Zn-Zr intermetallic compounds in Mg-Zn-Zr alloys.

Keywords: Mg-Zn-Zr alloys; mechanical properties; thermal conductivity; density functional theory

1. Introduction

Grain refinement is a metallurgical phenomenon that has been exploited in magnesium alloys to achieve desired microstructure and mechanical properties. Zirconium, a powerful grain refiner, has been widely used in magnesium alloys [1–3]. Magnesium-zinc-zirconium (ZK) alloys mainly refer to those containing zirconium or grain refined by zirconium, such as ZE41, ZK60, WE43, ML12, and ML10, as well as OS-1–3, and such like, and these commercial Mg-Zn-Zr alloys comprise the basis of the current magnesium alloy business. It was previously agreed that grain refinement of magnesium alloys by Zr was noticeable at low levels of soluble Zr [4], but the subsequently detailed examinations showed that both insoluble zirconium particles and zirconium dissolved in the melt played a role in grain refinement [5]. These conditions require that the magnesium alloys contain maximum soluble and undissolved Zr content. Meanwhile, a large amount of Zr content could lead to the formation of Zn-Zr intermetallic compounds in Mg-Zn-Zr alloys.

Based on the study of the composition and distribution of zirconium, Morozova and Mukhina [6] proposed that the highly dispersed particles of Zn_2Zr_3, ZnZr, and Zn_2Zr intermetallic compounds were the determining factors for the nano-structural mechanism of strengthening in the Mg-Zn-Zr system. Li et al. [7] proposed that the Mg-5Zn-2Gd-0.4Zr alloy (wt.%) showed a significant hardening response during aging, thus forming different morphologies, including ZnZr and Zn_2Zr phases. Although the $ZnZr_2$ and Zn_2Zr_3 phases do not belong to the ground state of the Zn-Zr system, they were dynamically

stable at 0 K using the harmonic approximation [8]. Recently, it was reported that Mg-Zn-Zr alloys were also prospective to be ideal thermal conductive material for application in LED light fixtures [1,9]. With the aging process, Li et al. [10] suggested that the thermal conductivity of Mg-2Zn-Zr alloy obviously increased due to the precipitation of Zn atoms from the α-Mg matrix, accompanied by the formation of Zn-Zr precipitations, such as ZnZr, Zn_2Zr, and Zn_2Zr_3. Similarly, Yamasaki and Kawamura [11] proposed the thermal conductivity of Mg-Zn-rare earth (RE) alloys exhibited higher thermal conductivity than their solution-treated counterparts due to the consumption of solute elements during the formation of the long-period stacking ordered phase (LPSO). Also, due to the formation of a rare-earth phase, the thermal conductivity of the Mg alloy was raised markedly with an increase in Sm content, which helped to dissolve the Zn atoms in the α-Mg matrix [12].

Laves $MgZn_2$ is known to be the most important strengthening phase in Mg-Zn-Zr alloys. Due to the importance of the strengthening effects of the $MgZn_2$ phase and the role of micro-alloying on precipitation strengthening, $MgZn_2$ has been studied extensively through theoretical calculations to experimental exploration [13–15]. By adding grain-refining elements, the density of aging precipitate $MgZn_2$ can be increased, thereby improving the mechanical properties of the alloy [15]. Meanwhile, it is also an effective way to dissolve the Zn atoms in the α-Mg matrix by forming the $MgZn_2$ phase. However, to our knowledge, theoretical research regarding mechanical properties and thermal conductivities of Zn-Zr intermetallic compounds compared with $MgZn_2$ are relatively scarce.

In addition, experimental information is quite limited in establishing phase/property relationships for these precipitations. Nevertheless, the first principles calculations may be an available approach to research these properties. Accordingly, the mechanical and thermal conductivity properties of ZnZr, Zn_2Zr, Zn_2Zr_3, and $MgZn_2$ have been conducted through the first-principles calculations. Generally, the minimum thermal conductivity can be used to identify candidate materials for high-temperature applications. In this contribution, the minimum thermal conductivity, according to the modified Clarke's model [16] is investigated for intermetallic compounds ZnZr, Zn_2Zr, and Zn_2Zr_3. In addition, the direction-dependent minimum thermal conductivity, based on the Cahill's model [17] has been further studied in-depth to understand the effect of the Zn-Zr precipitations on the thermal conductivity properties of Mg-Zn-Zr alloys. Undoubtedly, it is anticipated that the results will guide people's selections of the appropriate ZK alloys for different applications.

2. Computational Details

All calculations in this work were performed by using the Vienna ab initio simulation package code (VASP) [18] within the generalized gradient approximation (GGA) [19] of Perdew-Burke-Ernzerhof (PBE) [20] exchange correlation density functional. The electron configuration treated $3s^2$ as a valence state for Mg, $3d^{10}4s^2$ as a valence state for Zn, and $4s^24p^65s^24d^2$ for Zr, respectively. Extensive convergence tests suggested that the cutoff energy of 400 eV was enough for all phases in the calculations. The special points sampling integration was used over the Brillouin zone with $7 \times 7 \times 3$ and $8 \times 8 \times 8$ k-points using the Gamma-centered Monkhorst-Pack method [21] for $MgZn_2$ and the Zn-Zr system (including ZnZr, Zn_2Zr and Zn_2Zr_3), respectively, in geometry optimization. The convergence criterion of the Hellmane Feynman force was 0.01 eV/Å for complete relaxation of the atomic positions within the maximum stress on the atom of 0.02 GPa. The electronic iterations convergence was 1.0×10^{-5} eV for the total energy calculated together with first-order Methfessel-Paxton smearing with a width of 0.2 eV. Considering the unfilled electron of the *4d* shell of the transition metal Zr, the spin polarization was considered in the calculation with the initial magnetic moment 3 μ_B according to Hund rules.

For obtaining the equilibrium bulk modulus B_0 of the spin state at 0 K, the ground state energy E_0 as a function of the cell volume within the Birch-Murnaghan equation of states (EOS) [22] was applied. Meanwhile, in order to investigate chemical stability, the contribution of the lattice vibrations F_{vib} to the total Helmholtz free energy ($F = E_0 + F_{vib}$) was evaluated (it is worth noting that the contribution of the thermal electrons is negligible compared to lattice vibrations, and is therefore ignored in the

current work). For the sake of computational efficiency, the vibrational free energy was derived by using the Debye-Grüneisen [23] model as follows:

$$F_{\mathrm{vib}}(V,T) = \frac{9}{8}nk_{\mathrm{B}}\Theta + T\left[3\ln\left(1-e^{-\Theta/T}\right) - D(\Theta/T)\right] \quad (1)$$

where k_{B} is the Boltzmann constant and n is the number of atoms per formula unit. The Debye temperature Θ was obtained as proposed by using [24]:

$$\Theta_D = \frac{1}{K_{\mathrm{B}}}\left(6\pi^2 V^{1/2} n\right)^{1/3} f(\sigma)\sqrt{\frac{B_0}{M}} \quad (2)$$

where M is the molecular mass per primitive cell, and B_0 and σ are the static bulk modulus and Poisson ratio at the equilibrium geometry, respectively. The $f(\sigma)$ function is:

$$f(\sigma) = \left\{3\left[2\left(\frac{2}{3}\frac{(1+\sigma)}{(1-2\sigma)}\right)^{3/2} + \left(\frac{1}{3}\frac{(1+\sigma)}{(1-\sigma)}\right)^{3/2}\right]^{-1}\right\}^{1/3} \quad (3)$$

The elastic coefficients were determined by applying a set of given deformation with a finite value fitting the total energy of the crystal, as implemented by Mayer et al. [25]. In order to remain within the elastic limit of the selected phases, small strains up to ±2% at 0.5% interval were used.

3. Results and Discussion

3.1. Structure and Stability

Figure 1 shows the energy-volume fittings for ZnZr, Zn_2Zr, Zn_2Zr_3 at both no-spin and spin states, as well as $MgZn_2$ at a nonmagnetic state. It is clear that for energy that was dependent on the volume of the two states, the spin state was more energetically stable than the no-spin state for Zn-Zr intermetallic compounds, especially for the Zn_2Zr phase. Thus, in the following discussion, we focus on properties at the magnetic state. The optimized lattice constants at the ground state and the corresponding fitting B_0 for each Zn-Zr intermetallic compound are given in Table 1. As seen, the calculated lattice parameters of Zn-Zr intermetallic compounds and the $MgZn_2$ phase are in good agreement with the available calculated results. When comparing the equilibrium bulk moduli of these four intermetallic compounds, which could describe the stiffness of the crystal to the applied strain, it can be observed that the B_0 of the selected Zn-Zr compounds is interestingly larger than that of $MgZn_2$, which has generally been considered as the main strengthening phase in Mg-Zn alloys. We estimated the chemical stability based on the calculated Helmholtz free energy F (eV/atom) of Zn-Zr compounds. Generally speaking, these phases are thermodynamically stable due to negative Helmholtz free energy, which is considered to be a key factor for the alloys' synthesis and stabilization; the more negative it is, the more stable the structure. Furthermore, it has been shown from the Helmholtz free energy F that the thermodynamic stability sequence is Zn_2Zr_3 > ZnZr > Zn_2Zr > $MgZn_2$, and Zn_2Zr_3 is the most thermodynamically stable compound.

Table 1. The calculated lattice parameters at the ground state (a, c in Å, ρ in g/cm^3) and the fitting bulk modulus B_0 (GPa) at the spin state, as well as the Helmholtz free energy F (eV/atom) at 0 K. For $MgZn_2$, the B_0 responds to the no-spin state.

Species	Space Group	Lattice Parameters		ρ	B_0	F
		a	c			
ZnZr	$Pm\bar{3}m$	3.34 (3.34 [a])	-	7.00	107.11	−5.07
Zn_2Zr	$Fd\bar{3}m$	7.39 (7.40 [a])	-	7.31	104.47	−3.83
Zn_2Zr_3	$P4_2/mnm$	7.59 (7.63 [a])	6.83 (6.76 [a])	6.84	102.54	−5.71
$MgZn_2$	$P6_3/mmc$	5.23 (5.20 [b])	8.56 (8.54 [b])	5.17	63.69	−1.34

[a] From Reference [8]. [b] From Reference [26].

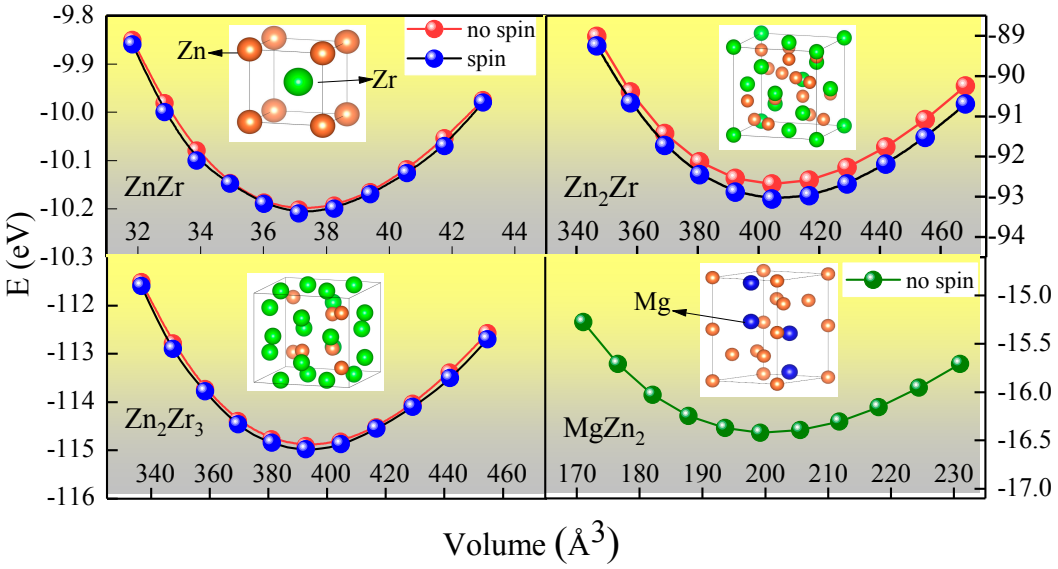

Figure 1. Total energy as a function of unit cell volume for ZnZr, Zn_2Zr, and Zn_2Zr_3 at both no-spin and spin states, as well as $MgZn_2$ at the nonmagnetic state.

3.2. Elastic Constants, Polycrystalline Moduli

The calculated elastic constants of the various phases are shown in Table 2. In reality, Zn-Zr intermetallic compounds exhibit much better resistance to deformation than $MgZn_2$ due to larger elastic constants; not only regarding C_{11} and C_{33} under uniaxial stress along the x or z axes, respectively, but also other compression moduli (C_{12} and C_{13}) and shear moduli (C_{44}, and C_{66}). At this point it may be clear that ZnZr, Zn_2Zr, and Zn_2Zr_3 are effective strengthening phases in Mg-Zn-Zr alloys, aside from $MgZn_2$. For hexagonal $MgZn_2$ and tetragonal Zn_2Zr_3 crystals $C_{11} = C_{22} \neq C_{33}$, the difference between C_{11} (C_{22}) and C_{33} indicates that the two crystals have relatively strong anisotropic elastic constants, resulting in the directional dependence of the moduli. Interestingly, for hexagonal $MgZn_2$ and tetragonal Zn_2Zr_3 crystals, the values of C_{33} is larger than that of C_{11}, implying that the chemical bonds in the direction of [001] are stronger than those along the direction of [100]. The stronger chemical bonds result in hard compressing under uniaxial stress along the z axes. Moreover, the relatively large difference between C_{11} and C_{33} of $MgZn_2$ implies that there is greater anisotropy on the directional dependence of the moduli than Zn_2Zr_3.

Table 2. The calculated independent elastic constants (GPa) of Zn-Zr intermetallic compounds and $MgZn_2$ using the strain-energy method with other calculated (Cal.) and experimental (Exp.) data.

Species	Reference	C_{ij}					
		C_{11}	C_{12}	C_{13}	C_{33}	C_{44}	C_{66}
ZnZr	This work	134.04	91.82	-	-	72.96	-
	Cal. [27]	141.00	91.00	-	-	71.00	-
Zn_2Zr	This work	183.72	68.59	-	-	62.36	-
Zn_2Zr_3	This work	145.94	90.00	73.72	155.22	31.76	47.00
$MgZn_2$	This work	93.30	60.88	32.75	109.53	24.76	-
	Cal. [28]	91.25	87.27	28.62	147.59	20.21	-
	Exp. [29]	107.25	45.45	27.43	126.40	27.70	–

In order to synthetically estimate the mechanical properties, the polycrystalline bulk modulus B, shear modulus G, and Young's modulus E were calculated via Voigt-Reuss-Hill approximations [30–32]. Figure 2 summarizes the calculated mechanical performance parameters. Notably, the B values of ZnZr, Zn_2Zr, and Zn_2Zr_3 are close, and are all larger than that of $MgZn_2$. The larger B values responded to the stronger capacity of the resist deformation, reflecting the good resistance of the selected Zn-Zr intermetallic compounds to deformation. Meanwhile, the B values of all considered intermetallic compounds are in good agreement with the fitting bulk modulus, B_0. The shear modulus G of the system in descending order is: Zn_2Zr > ZnZr > Zn_2Zr_3 > $MgZn_2$. It is clear that the Young's modulus E has the same order as the shear modulus G, suggesting that Young's modulus E of the considered polycrystalline materials is more sensitive to the shear modulus than the bulk modulus. Relatively larger mechanical parameters, including bulk modulus B, shear modulus G, and Young's modulus E, prove that Zn_2Zr has outstanding mechanical properties and pronounced strengthening effects among all strengthening phases. In contrast, the lowest B/G value 1.76 reveals its brittle characteristics relative to other phases, although the material behaves as ductile when the B/G ratio >1.75 [33]. Analysis of Figure 2 thus allows us to conclude that ZnZr and Zn_2Zr_3 serve to combine the natures of high strength and great ductility.

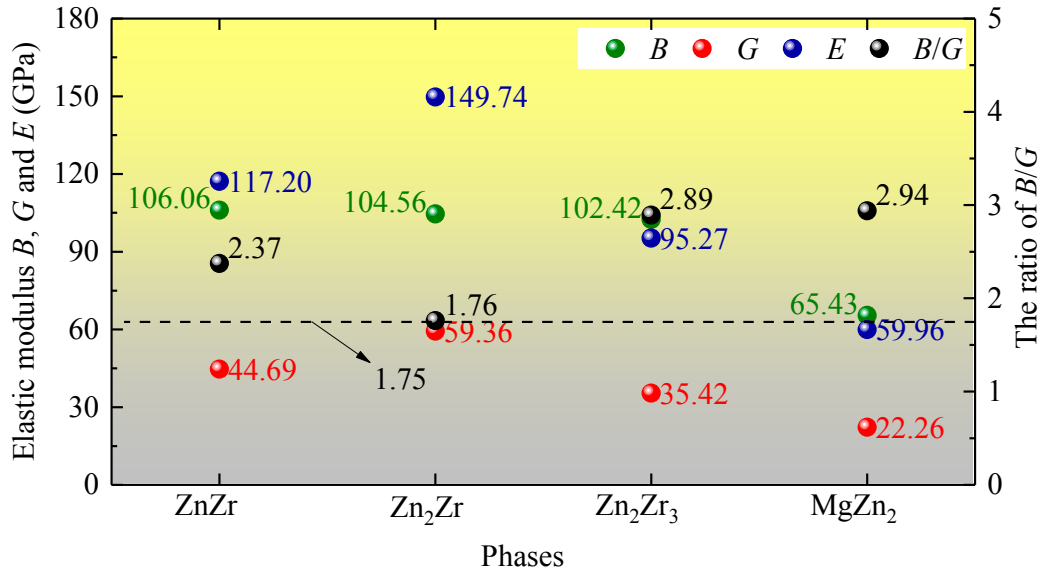

Figure 2. Calculated mechanical properties, including bulk modulus B, shear modulus G, and Young's modulus E, as well as B/G values for ZnZr, Zn_2Zr, Zn_2Zr_3, and $MgZn_2$.

3.3. Electronic Structures

To gain further insight into the reasons for the Zn-Zr system strengthening, the electron localization function (ELF) [34] was applied to assist in identifying the distribution of the charges and the bonding condition. As a general rule, the ELF value is on the range $0 \leq \mathrm{ELF} \leq 1$, where ELF = 0, 1 corresponds to the completely delocalized state and the perfect localization, respectively. The electron localization functions on the (110) plane for all selected intermetallic compounds are presented in Figure 3. Clearly, there are obvious ionic characteristics in ZnZr, Zn_2Zr, and Zn_2Zr_3 intermetallic compounds due to the delocalization around Zn and localization around Zr. Meanwhile, Zn-Zn and Zr-Zr present typical metal bond characteristics because of the even distribution of charges between the component atoms. In contrast, Mg-Zn bonds show covalent characteristics based on the apparent accumulation of charge distribution between Mg and Zn atoms in $MgZn_2$ alloys. This result is consistent with the investigation of Reference [35], where more hybridized peaks between Mg p and Zn p appear near the Fermi level, indicating the presence of strong covalent bonding. Based on the above discussion, the bonding characteristics in Zn-Zr and $MgZn_2$ intermetallic compounds play a role in determining a ductile or brittle nature, meaning that ionic bonds in Zn-Zr intermetallic compounds cause them to have lower ductility than $MgZn_2$. In addition, for Zn-Zr intermetallic compounds, the strength of the ionic bond was also compared based on the result of charge transfer using the Bader charge analysis. For a reasonable and intuitive comparison, the average charge transfer amount of per Zr atom (e/atom) in Zn-Zr intermetallic compounds could be used as a basis, and the descending order is: Zn_2Zr (1.01) > ZnZr (0.95) > Zn_2Zr_3 (0.72). From the perspective of ionic bonds, the strength of the Zn_2Zr phase is stronger than ZnZr and Zn_2Zr_3, which is entirely consistent with the above elastic moduli results.

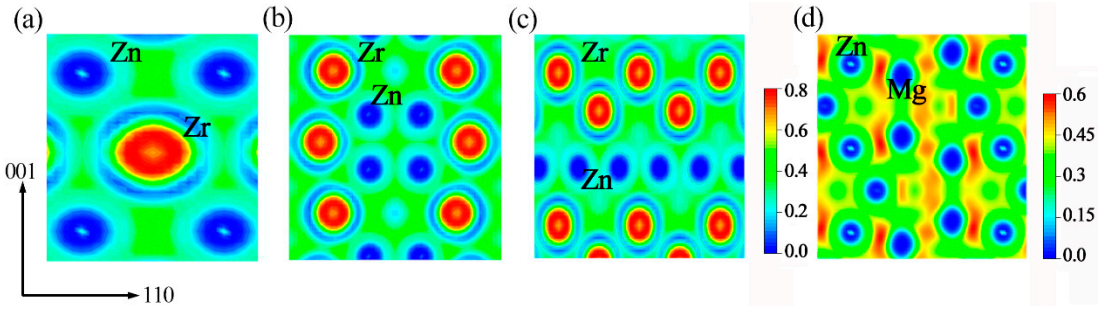

Figure 3. The contour line diagrams of the electron localization function (ELF) electronic distributions for Zn-Zr and $MgZn_2$ intermetallic compounds on the (110) plane—namely, ZnZr (**a**), Zn_2Zr (**b**), Zn_2Zr_3 (**c**), and $MgZn_2$ (**d**). The interval between the two nearest contour lines is 0.2 and 0.15 for the two systems, respectively.

3.4. Minimum Thermal Conductivity and Anisotropy

It is well-known that thermal conductivity is inversely proportional to temperature. At elevated temperatures, the thermal conductivity will decrease to a limit value considered as the minimum thermal conductivity, which can be developed to identify candidate materials for high-temperature applications [36,37]. For the purpose of precisely calculating the minimum thermal conductivity of selected Zn-Zr and $MgZn_2$ intermetallic compounds with anisotropic chemical bonds, the modified Clarke relation by Liu et al. [16] was used as defined:

$$k_{\min} \rightarrow k_{\mathrm{B}} \nu_{\mathrm{m}} \left(\frac{M}{npN_{\mathrm{A}}} \right)^{-2/3} \tag{4}$$

where k_B is the Boltzmann's constant, v_m is the average sound velocity, N_A is Avogadro's number, ρ is the density, M is the molecular weight, and n is the number of atoms in the molecule. The average sound velocity v_m is given by [38,39]:

$$v_m = \left[\frac{1}{3}\left(\frac{2}{v_t^3} + \frac{1}{v_l^3}\right)\right]^{-1/3} \tag{5}$$

$$v_t = \sqrt{\frac{G}{\rho}} \tag{6}$$

$$v_l = \sqrt{\frac{B + 4/3G}{\rho}} \tag{7}$$

where B and G are the bulk modulus and shear modulus, respectively. Using Liu's model, the minimum thermal conductivity of ZnZr, Zn_2Zr, Zn_2Zr_3, and $MgZn_2$ is 0.48, 0.67, 0.68, and 0.49 ($W \cdot m^{-1} \cdot K^{-1}$), respectively. Since the values of the minimum thermal conductivities of the Zn-Zr intermetallic compounds such as Zn_2Zr and Zn_2Zr_3 are far larger than $MgZn_2$, it can be proved that the thermal conductivity of the Mg-Zn-Zr alloy will be markedly improved as the precipitation of Zn atoms from the α-Mg matrix form Zn-Zr intermetallic compounds other than $MgZn_2$. Meanwhile, Zn_2Zr_3, with maximum thermal conductivity, can be considered as the most important contribution to the total thermal conductivity due to its minimum Helmholtz free energy, which is considered to be a key factor for the alloys to be formed. However, for ZnZr, the difference in the minimum thermal conductivity between them could still be ignored.

Furthermore, an important question to ask is how the minimum thermal conductivity along a different direction can affect the overall minimum thermal conductivity. To clarify this point, the directional dependence of the minimum thermal conductivity can be computed from the quasi-transverse or quasi-longitudinal sound velocities and the number density of atoms per mole (n) of the compound, according to Cahill's model [17]:

$$K_{min} = \frac{k_B}{2.48} n^{2/3} (v_l + v_{t1} + v_{t2}) \tag{8}$$

for tetragonal Zn_2Zr_3 crystal structure symmetry, the acoustic velocities can simply be written as:

$$[100] = [010] v_l = \sqrt{C_{11}/\rho};\ [001] v_{t1} = \sqrt{C_{44}/\rho};\ [010] v_{t2} = \sqrt{C_{66}/\rho}$$

$$[001] v_l = \sqrt{C_{33}/\rho};\ [100] v_{t1} = [010] v_{t2} = \sqrt{C_{66}/\rho}$$

$$[110] v_l = \sqrt{(C_{11} + C_{12} + 2C_{66})/2\rho};\ [001] v_{t1} = \sqrt{C_{44}/\rho};\ [0\bar{1}0] v_{t2} = \sqrt{(C_{11} - C_{12})/2\rho}$$

for hexagonal $MgZn_2$:

$$[100] v_l = \sqrt{(C_{11} - C_{12})/2\rho};\ [010] v_{t1} = \sqrt{C_{11}/\rho};\ [010] v_{t2} = \sqrt{C_{44}/\rho}$$

$$[001] v_l = \sqrt{C_{33}/\rho};\ [100] v_{t1} = [010] v_{t2} = \sqrt{C_{44}/\rho}$$

for cubic ZnZr and Zn_2Zr:

$$[100] = [010] = [001] v_l = \sqrt{C_{11}/\rho};\ [010] v_{t1} = [010] v_{t2} = \sqrt{C_{44}/\rho}$$

$$[110] v_l = \sqrt{(C_{11} + C_{12} + 2C_{44})/2\rho};\ [1\bar{1}0] v_{t1} = \sqrt{(C_{11} - C_{12})/2\rho};\ [001] v_{t1} = \sqrt{C_{44}/\rho}$$

The calculated acoustic velocities along different crystal directions are shown in Figure 4. It is clear that Zn_2Zr exhibits relatively little deviations in terms of all considered acoustic velocities due to

the small variation in elastic constants. All Zn-Zr intermetallic compounds present better symmetry results along the [100], [010], and [001] directions compared with $MgZn_2$, and this may be the result of its hexagonal symmetry. Interestingly, the difference between quasi-transverse and quasi-longitudinal acoustic velocities for each Zn-Zr crystal structure along the [110] direction are most pronounced, indicating that the most diverse chemical bonds are in this direction. However, the quasi-longitudinal sound velocity of all Zn-Zr intermetallic compounds in the [110] direction are closest to each other, probably because they exhibit similar ionic bonds in the [110] direction.

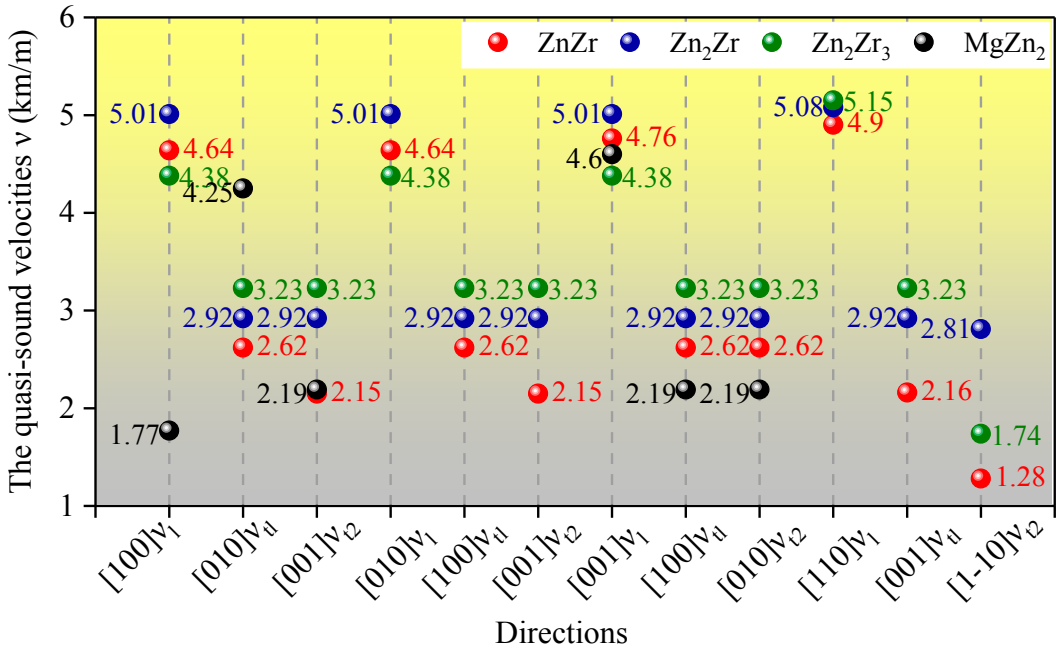

Figure 4. The calculated transverse and longitudinal acoustic velocities along different directions for ZnZr, Zn_2Zr, Zn_2Zr_3, and $MgZn_2$.

In addition, the theoretical minimum thermal conductivities along different principle directions can be obtained using the acoustic velocities, as shown in Figure 5. For all considered intermetallic compounds, the directional dependence of the minimum thermal conductivity obtained in the present calculation is around 30% higher than those obtained by the Liu relation. Nevertheless, by comparing the values of minimum thermal conductivity in different directions, we can still understand the anisotropy of the minimum thermal conductivity to some extent. As can be observed, the minimum thermal conductivities of the ZnZr, Zn_2Zr, and $MgZn_2$ intermetallic compounds are the same in the three principle axis directions, indicating that the limit of thermal conductivity along the x, y, and z axes are directionally insensitive. Compared with ZnZr, Zn_2Zr, and $MgZn_2$, the minimum thermal conductivity of Zn_2Zr_3 along the z axis is higher than the x and y axes. What is striking in this figure is the minimum thermal conductivity along the [110] direction. It can be seen that the value of minimum thermal conductivity along the [110] direction is the smallest for all considered directions, indicating that Zn-Zr ionic bonding in the [110] direction will greatly affect the thermal conductivity at high temperatures, which will result in slower heat dissipation in the [110] direction. The minimum thermal conductivity in the [110] direction will be a crucial factor when considering the minimum thermal conductivity for the selected Zn-Zr intermetallic compounds, especially for Zn_2Zr_3. This fact definitely indicates that the bonding anisotropy, reflected in the elastic constant anisotropy, leads to anisotropy in the high-temperature limit of thermal conductivity—that is, the minimum thermal conductivity.

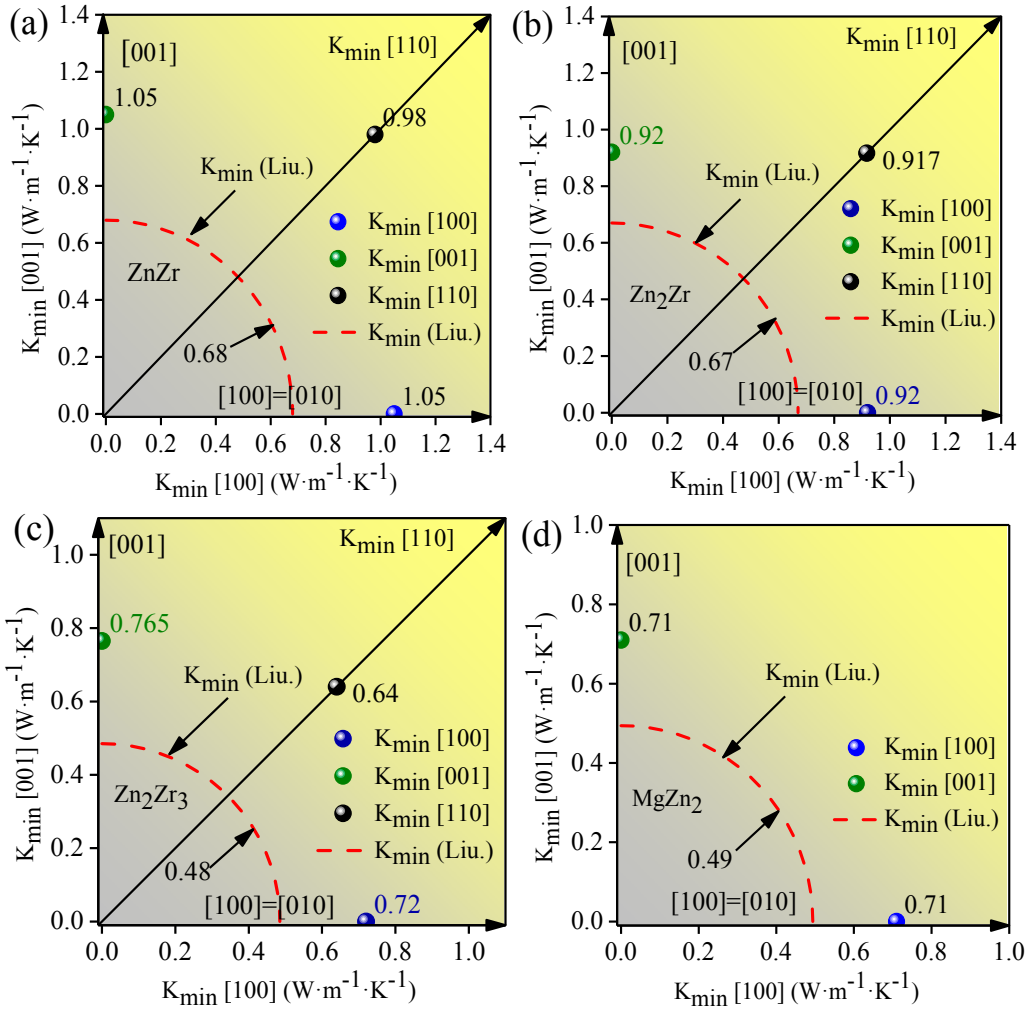

Figure 5. The minimum thermal conductivities along different principal directions of alloys, evaluated using Cahill's equation and Liu's model. (**a**) ZnZr; (**b**) Zn_2Zr; (**c**) Zn_2Zr_3 and (**d**) $MgZn_2$.

4. Conclusions

In summary, the structural stability, mechanical properties, bonding characteristics, and minimum thermal conductivity for the intermetallic compounds ZnZr, Zn_2Zr, Zn_2Zr_3, and $MgZn_2$ have been investigated by first-principles calculations. Moreover, the crystal direction/minimum thermal conductivity relationship of the materials were also established.

Based on the difference between C_{11} and C_{33}, $MgZn_2$ was found to possess greater anisotropy on the directional dependence of the modulus than Zn_2Zr_3. ZnZr and Zn_2Zr_3 was found to combine the natures of high strength and great ductility. Strong ionic bonds in ZnZr, Zn_2Zr, and Zn_2Zr_3 was found to lead to the characteristics of a higher modulus but lower ductility than $MgZn_2$. Furthermore, the strength of the Zn_2Zr phase was found to be stronger than ZnZr and Zn_2Zr_3 based on the maximum charge transfer using Bader's charge analysis. Based on the calculated minimum thermal conductivities of the intermetallic compounds ZnZr, Zn_2Zr, Zn_2Zr_3, and $MgZn_2$, we conclude that the thermal conductivity of the Mg-Zn-Zr alloy will be markedly improved as the precipitation of Zn atoms from the α-Mg matrix help to form Zn-Zr binary alloys. However, the minimum thermal conductivity along the [110] direction may serve to be a crucial limit.

Author Contributions: Conceptualization, Y.Z. and S.W.; Methodology, S.W.; Software, Y.Z.; Validation, Y.Z., S.W. and H.H.; Formal Analysis, S.W.; Investigation, S.W.; Resources, Y.Z.; Data Curation, H.G.; Writing-Original Draft Preparation, S.W.; Writing-Review & Editing, Y.Z.; Visualization, F.L.; Supervision, H.H.; Project Administration, H.H.; Funding Acquisition, Y.Z.

Funding: This work is supported by the National Natural Science Foundation of China (Nos. U1610123, 51674226, 51574207, 51574206, 51774254, 51774253, 51701187), Science and Technology Major Project of Shanxi Province (No. MC2016-06).

Conflicts of Interest: The authors declare that they have no competing interests.

References

1. Robson, J.D.; Paa-Rai, C. The interaction of grain refinement and ageing in magnesium-zinc-zirconium (ZK) alloys. *Acta Mater.* **2015**, *95*, 10–19. [CrossRef]
2. Stjohn, D.H.; Qian, M.; Easton, M.A.; Cao, P.; Hildebrand, Z. Grain refinement of magnesium alloys. *Metall. Mater. Trans. A* **2005**, *36*, 1669–1679. [CrossRef]
3. Kunčická, L.; Kocich, R. Comprehensive Characterisation of a Newly Developed Mg–Dy–Al–Zn–Zr Alloy Structure. *Metals* **2018**, *8*, 73. [CrossRef]
4. Qian, M.; Stjohn, D.H.; Frost, M.T. Heterogeneous nuclei size in magnesium–zirconium alloys. *Scr. Mater.* **2004**, *50*, 1115–1119. [CrossRef]
5. Qian, M.; Stjohn, D.H.; Frost, M.T. Zirconium alloying and grain refinement of magnesium alloys. *Magnes. Technol.* **2003**, *2003*, 209–214.
6. Morozova, G.I.; Mukhina, I.Y. Nanostructural hardening of cast magnesium alloys of the Mg-Zn-Zr system. *Met. Sci. Heat Treat.* **2011**, *53*, 3–7. [CrossRef]
7. Li, J.H.; Barrirero, J.; Sha, G.; Aboulfadl, H.; Mücklich, F.; Schumacher, P. Precipitation hardening of an Mg-5Zn-2Gd-0.4Zr (wt. %) alloy. *Acta Mater.* **2016**, *108*, 207–218. [CrossRef]
8. Arroyave, R.; van de Walle, A.; Liu, Z.K. First-principles calculations of the Zn-Zr system. *Acta Mater.* **2006**, *54*, 473–482. [CrossRef]
9. Wu, R.; Yan, Y.; Wang, G.; Murr, L.E.; Han, W.; Zhang, Z.; Zhang, M. Recent progress in magnesium-lithium alloys. *Int. Mater. Rev.* **2014**, *60*, 65–100. [CrossRef]
10. Li, B.; Hou, L.; Wu, R.; Zhang, J.; Li, X.; Zhang, M.; Dong, A.; Sun, B. Microstructure and thermal conductivity of Mg-2Zn-Zr alloy. *J. Alloys Compd.* **2017**, *7221*, 772–777. [CrossRef]
11. Yamasaki, M.; Kawamura, Y. Thermal diffusivity and thermal conductivity of Mg-Zn-rare earth element alloys with long-period stacking ordered phase. *Scr. Mater.* **2009**, *60*, 264–267. [CrossRef]
12. Yang, C.; Pan, F.; Chen, X.; Luo, N.; Han, B.; Zhou, T. Thermal conductivity and mechanical properties of Sm-containing Mg-Zn-Zr alloys. *Mater. Sci. Technol.* **2018**, *34*, 138–144. [CrossRef]
13. Li, X.D.; Ma, H.T.; Dai, Z.H.; Qian, Y.C.; Hu, L.J.; Xie, Y.P. First-principles study of coherent interfaces of Laves-phase $MgZn_2$ and stability of thin $MgZn_2$ layers in Mg-Zn alloys. *J. Alloys Compd.* **2017**, *696*, 109–117. [CrossRef]
14. Tsuru, T.; Yamaguchi, M.; Ebihara, K.; Itakura, M.; Shiihara, Y.; Matsuda, K. First-principles study of hydrogen segregation at the $MgZn_2$ precipitate in Al-Mg-Zn alloys. *Comput. Mater. Sci.* **2018**, *148*, 301–306. [CrossRef]
15. Qian, M.; Das, A. Grain refinement of magnesium alloys by zirconium: Formation of equiaxed grains. *Scr. Mater.* **2006**, *54*, 881–886. [CrossRef]
16. Liu, B.; Wang, J.Y.; Li, F.Z.; Zhou, Y.C. Theoretical elastic stiffness, structural stability and thermal conductivity of $La_2T_2O_7$ (T = Ge, Ti, Sn, Zr, Hf) pyrochlore. *Acta Mater.* **2010**, *58*, 4369–4377. [CrossRef]
17. Cahill, D.G.; Watson, S.K.; Pohl, R.O. Lower limit to the thermal conductivity of disordered crystals. *Phys. Rev. B Condens. Matter* **1992**, *46*, 6131–6140. [CrossRef] [PubMed]
18. Kresse, G.; Furthmüller, J. Efficient iterative schemes for ab initio total-energy calculations using a plane-wave basis set. *Phys. Rev. B Condens. Matter* **1996**, *54*, 11169–11186. [CrossRef] [PubMed]
19. Perdew, J.P.; Chevary, J.A.; Vosko, S.H.; Jackson, K.A.; Pederson, M.R.; Singh, D.J. Atoms, molecules, solids, and surfaces: Applications of the generalized gradient approximation for exchange and correlation. *Phys. Rev. B Condens. Matter* **1993**, *46*, 6671–6687. [CrossRef]
20. Perdew, J.P.; Burke, K.; Ernzerhof, M. Generalized gradient approximation made simple. *Phys. Rev. Lett.* **1996**, *77*, 3865–3868. [CrossRef] [PubMed]
21. Monkhorst, H.J. Special points for Brillouin-zone integrations. *Phys. Rev. B Condens. Matter* **1976**, *16*, 1748–1749. [CrossRef]

22. Otero-de-la-Roza, A.; Abbasi-Pérez, D.; Luaña, V. Gibbs2: A new version of the quasiharmonic model code. *II. Models for solid-state thermodynamics, features and implementation. Comput. Phys. Commun.* **2011**, *182*, 2232–2248.
23. Moruzzi, V.L.; Janak, J.F.; Schwarz, K. Calculated thermal properties of metals. *Phys. Rev. B* **1988**, *37*, 790–799. [CrossRef]
24. Álvarez Blanco, M. Métodos cuánticos locales para la simulación de materiales iónicos. Fundamentos, algoritmos y aplicaciones. Ph.D. Thesis, Universidad de Oviedo, Asturias, Spain, July 1997.
25. Mayer, B.; Anton, H.; Bott, E.; Methfessel, M.; Sticht, J.; Harris, J.; Schmidt, P.C. Ab-initio calculation of the elastic constants and thermal expansion coefficients of Laves phases. *Intermetallics* **2003**, *11*, 23–32. [CrossRef]
26. Wang, S.; Zhao, Y.; Hou, H.; Wen, Z.; Zhang, P.; Liang, J. Effect of anti-site point defects on the mechanical and thermodynamic properties of $MgZn_2$, $MgCu_2$ Laves phases: A first-principle study. *J. Solid State Chem.* **2018**, *263*, 18–23. [CrossRef]
27. De, J.M.; Chen, W.; Angsten, T.; Jain, A.; Notestine, R.; Gamst, A. Charting the complete elastic properties of inorganic crystalline compounds. *Sci. Data* **2015**, *2*, 150009.
28. Mao, P.; Yu, B.; Liu, Z.; Wang, F.; Ju, Y. First-principles calculations of structural, elastic and electronic properties of AB2 type intermetallics in Mg-Zn-Ca-Cu alloy. *J. Magnes. Alloys* **2013**, *1*, 256–262. [CrossRef]
29. Seidenkranz, T.; Hegenbarth, E. Single-crystal elastic constants of $MgZn_2$ in the temperature range from 4.2 to 300 K. *Phys. Status Solidi A* **1976**, *33*, 205–210. [CrossRef]
30. Voigt, W. *Lehrbuch der Kristallphysik*; Teubner: Leipzig, Germany, 1928.
31. Reuss, A. Berechnung der Fließgrenze von Mischkristallen auf Grund der Plastizitätsbedingung für Einkristalle. *J. Appl. Math. Mech.* **1929**, *9*, 49–58. [CrossRef]
32. Hill, R. The Elastic Behaviour of a Crystalline Aggregate. *Proc. Phys. Soc. Sect. A* **2002**, *65*, 349–354. [CrossRef]
33. Mohri, T.; Chen, Y.; Kohyama, M.; Ogata, S.; Saengdeejing, A.; Bhattacharya, S.K. Mechanical properties of Fe-rich Si alloy from Hamiltonian. *NPJ Comput. Mater.* **2017**, *3*, 10. [CrossRef]
34. Becke, A.D.; Edgecombe, K.E. A simple measure of electron localization in atomic and molecular systems. *J. Chem. Phys.* **1990**, *92*, 5397–5403. [CrossRef]
35. Shao, L.; Shi, T.T.; Zheng, J.; Wang, H.C.; Pan, X.Z.; Tang, B.Y. First-principles study of point defects in C14 $MgZn_2$ Laves phase. *J. Alloys Compd.* **2016**, *654*, 475–481. [CrossRef]
36. Tadano, T.; Tsuneyuki, S. Quartic Anharmonicity of Rattlers and Its Effect on Lattice Thermal Conductivity of Clathrates from First Principles. *Phys. Rev. Lett.* **2018**, *120*, 105901. [CrossRef] [PubMed]
37. Wang, C.; Wang, H.; Chen, Y.B.; Yao, S.H.; Zhou, J. First-principles study of lattice thermal conductivity in $ZrTe_5$ and $HfTe_5$. *J. Appl. Phys.* **2018**, *123*, 175104. [CrossRef]
38. Poirier, P.J. *Introduction to the Physics of the Earth's Interior*, 2nd ed.; Cambridge University Press: Cambridge, UK, 2000.
39. Anderson, O.L. A Simplified Method for Calculating the Debye Temperature from Elastic Constants. *J. Phys. Chem. Solids* **1963**, *24*, 909–917. [CrossRef]